Visualizing the melting of periodic lattice distortions in a complex 2D charge density wave material via MeV-scale ultrafast electron diffraction

Siddiqui, Khalid, Durham, Daniel, Cropp, Frederick, Rajpurohit, Sangeeta, Ophus, Colin, et al.

Khalid M. Siddiqui, Daniel B. Durham, Frederick Cropp, Sangeeta Rajpurohit, Colin Ophus, Yanglin Zhu, Johan D. Carlström, Camille Stavrakas, Zhiqiang Mao, Archana Raja, Pietro Musumeci, Liang Z. Tan, Andrew M. Minor, Robert A. Kaindl, Daniele Filippetto, "Visualizing the melting of periodic lattice distortions in a complex 2D charge density wave material via MeV-scale ultrafast electron diffraction," Proc. SPIE 11684, Ultrafast Phenomena and Nanophotonics XXV, 116840A (5 March 2021); doi: 10.1117/12.2577621

SPIE.

Event: SPIE OPTO, 2021, Online Only

Visualizing the melting of periodic lattice distortions in a complex 2D charge density wave material via MeV-scale ultrafast electron diffraction

Khalid M. Siddiqui[a], Daniel B. Durham[b,c], Frederick Cropp[d,e], Sangeeta Rajpurohit[f], Colin Ophus[f], Yanglin Zhu[g], Johan D. Carlström[f], Camille Stavrakas[f], Zhiqiang Mao[g], Archana Raja[f], Pietro Musumeci[d], Liang Z. Tan[f], Andrew M. Minor[b,c], Robert A. Kaindl[a,h], and Daniele Filippetto[e]

[a]Materials Sciences Division, Lawrence Berkeley National Laboratory, Berkeley, CA 94720, USA
[b]National Center for Electron Microscopy, Molecular Foundry, Lawrence Berkeley National Laboratory, Berkeley, CA 94720, USA
[c]Department of Materials Science and Engineering, University of California, Berkeley, Berkeley, California, 94720, USA
[d]Department of Physics and Astronomy, University of California, Los Angeles, Los Angeles, California 90095, USA
[e]Accelerator Technology and Applied Physics Division, Lawrence Berkeley National Laboratory, One Cyclotron Road, Berkeley, California 94720, USA
[f]Molecular Foundry, Lawrence Berkeley National Laboratory, Berkeley, CA 94720, USA
[g]Department of Physics, The Pennsylvania State University, University Park, PA 16802, USA
[h]Department of Physics, Arizona State University, Tempe, AZ 85287,USA

ABSTRACT

We discuss our experiments that apply ultrafast electron diffraction (UED) to study structural dynamics of the phase transition in single crystal tantalum ditelluride, $TaTe_2$, a quasi-2D quantum material which exhibits a trimer superstructure at cryogenic temperatures. Intense near-infrared (NIR) pulses at 1030 nm are employed to quench the low temperature, atomically ordered state and the process is captured by ultrashort bunches of electrons as a function of pump-probe time delay. The diffraction signatures of the trimer superstructure recover on picosecond time scales. These measurements of $TaTe_2$ underscore moreover the applicability of the HiRES UED beamline at Lawrence Berkeley National Laboratory (LBNL) to probe ultrafast structural dynamics of complex materials.

Keywords: ultrafast electron diffraction, 2D materials, relativistic electron bunches, tantalum ditelluride, photo-induced phase transition, charge density waves, trimerization

1. INTRODUCTION

Symmetry-breaking phase transitions are a hallmark of layered quantum materials resulting from strong correlations between electronic, orbital, spin, and lattice degrees of freedom and the intricate balance between them.[1] One consequence of this is that many new states of the same system can emerge, often with unique properties.[2] Examples of systems that undergo spontaneous symmetry-breaking phase transitions leading to genesis of exotic states include high-temperature superconductors,[3] charge-density wave (CDW) materials,[4] multiferroics[5] and topological insulators.[6] Controlling the process in these materials is a very attractive endeavor for applications such as robust memory storage devices and photoswitches[7,8] and has been subject to intense research.[9] Tied

E-mail: dfilippetto@lbl.gov
E-mail: kaindl@asu.edu

Ultrafast Phenomena and Nanophotonics XXV, edited by Markus Betz, Abdulhakem Y. Elezzabi,
Proc. of SPIE Vol. 11684, 116840A · © 2021 SPIE · CCC code: 0277-786X/21/$21
doi: 10.1117/12.2577621

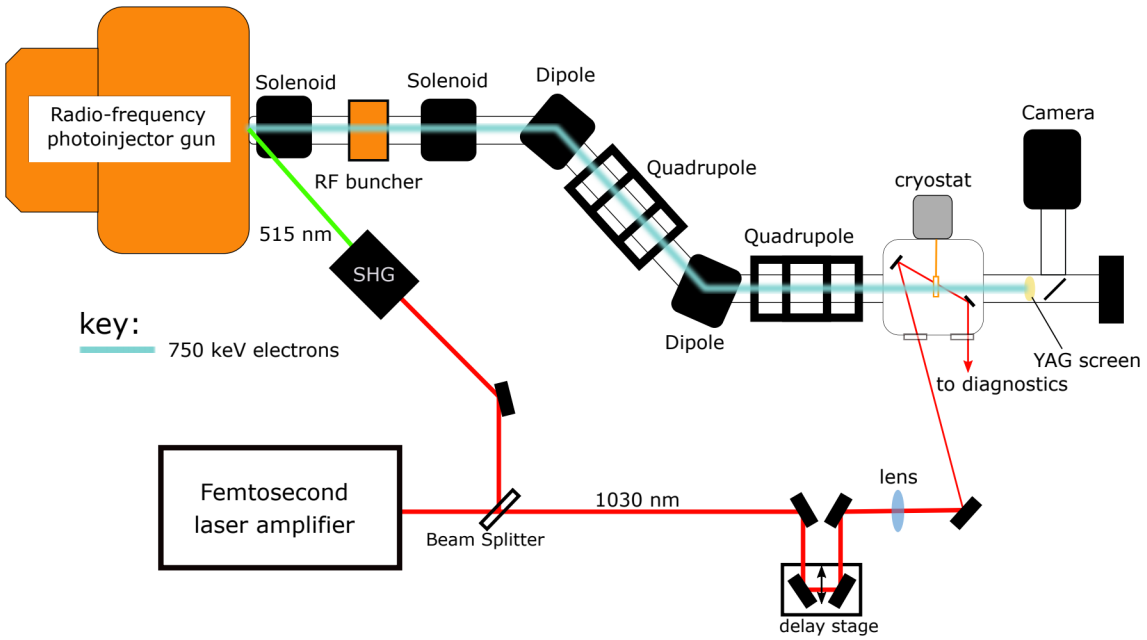

Figure 1. Schematic of the UED setup. Relativistic MeV-scale electron bunches produced by the LBNL HiRES instrument are used to monitor structural changes following pump excitation.

to this goal is the need to understand at the fundamental level processes that are responsible for the exotic phenomena. This forms one of the grand challenges in condensed matter physics, which is to resolve the dynamics of emerging quantum materials. Development of advanced ultrafast tools has enabled this with increasingly sophisticated experiments being performed of which some have led to observations of hidden metastable phases[10] as well as light-induced superconductivity when the system is driven out-of-equilibrium.[11] Usually, changes in the electronic structure or the material dielectric response are measured, but strong couplings means that the lattice degree of freedom is also affected. In order to follow atomically-resolved lattice dynamics on ultrafast timescales, pump-probe techniques employing structural probes such as electrons or x-rays are required.

Here, we are interested in ultrafast dynamics of an intriguing 2D material, 1T'-$TaTe_2$ belonging to the 1T-$TaSe_{2-x}Te_x$ family of compounds. This material is characterized by a distorted monoclinic crystal symmetry and undergoes a first-order phase transition to an atomically ordered state involving clustering of metal atoms into trimer chains below 174 K.[12–15] We apply ultrafast electron diffraction to study $TaTe_2$ under cryogenic conditions, which reveals picosecond-scale, reversible photoswitching of this trimer order.[16]

2. METHODS

The UED studies were carried out at the High Repetition-rate Electron Scattering (HiRES) facility at LBNL.[17,18] Electrons are well-suited for sensitive studies of long-range order because they are a direct probe of the lattice through their interaction with the electrostatic potential and their high scattering cross sections.[19] A schematic of the experimental setup at LBNL is illustrated in Fig. 1. A commercial high-power femtosecond fiber laser (50 W) provides the necessary laser output for experiments at 1030 nm, which is split into pump and probe arms. In the probe line, the beam is frequency-doubled to 515 nm after being focused inside a thick beta-Barium Borate (BBO) crystal setup for non-critical phase matching. A portion of this beam is imaged onto a semiconducting photocathode with work function in the vicinity of green, 515 nm light for electron generation. The electrons are accelerated and travel towards the sample chamber located down steam of the radio-frequency electron gun. The electron energy is ~750 keV corresponding to $\lambda = 0.01$ Å de Broglie wavelength, and the alignment and beam size are controlled by the beamline electron optics. The relativistic electrons enter the sample chamber and impinge on the sample which is cooled by a closed-cycle a vibrationally-isolated liquid helium cryostat. Most electrons pass through the sample without being scattered, whereas a small fraction that is scattered makes up

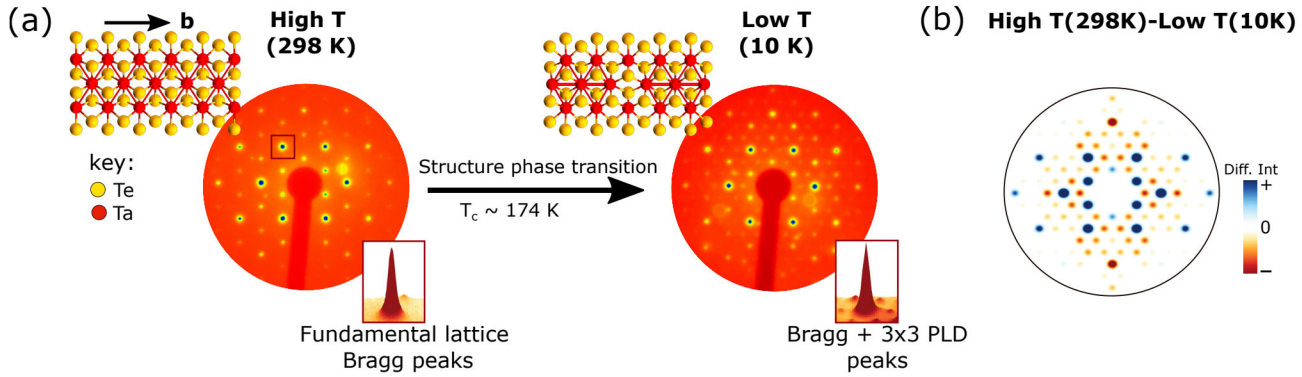

Figure 2. (a). Measured electron diffraction patterns at HiRES facility at different temperatures and the corresponding crystal structures of $TaTe_2$ (b). Difference pattern between the high-T and low-T structures representing the signature of low-T $\rightarrow$ high-T phase transition.

the diffraction signal, formed on a cerium-doped YAG scintillator crystal. A CCD camera records the diffraction patterns and stores the data in a computer for later processing.

In the pump arm, the laser beam is sent through an optical delay line and into the sample chamber and directed towards the sample holder as depicted in Fig. 1. The pump beam has a rough diameter of 750 μm^2 full-width-at-half-maximum (FWHM).

All UED experiments presented here were performed at 500 Hz effective repetition rate and a sample holder temperature of 10 K. For each pump-probe delay, 10 frames with the pump beam off and 10 frames with the pump on were acquired.

2.1 Sample preparation

Samples for the experiments were synthesized as single crystals using raw material (Tantalum (Ta) and Tellurium (Te) powder) and chemical vapor transport (CVT) technique.[20] A set ratio of Ta and Te was mixed in a sealed quartz tube at 850 ^oC with iodine as the transport agent. Plate-like flakes of $TaTe_2$ of about 1-1.5 mm^2 size were produced and later exfoliated repeatedly using the scotch tape method and transferred onto polydimethylsiloxane (PDMS) stamps. They were subsequently transferred onto a silicon nitride (SiN) membrane of 20 nm thickness and window size of 30 $\mu m \times 30$ μm by pressing the stamp against the membrane and very slowly releasing it (dry transfer method[21]). Atomic force microscopy (AFM) displayed a very flat topography, with slight rippling of $\sigma = 6.5$ mrad, where σ is the distribution of tilt angles on sample surface and sample thickness of 60 nm.

3. RESULTS

3.1 Equilibrium structures

We measured static electron diffraction patterns by looking along the $[10\bar{1}]$ zone axis of the layered structure to expose the symmetry of $TaTe_2$ at room temperature (high-T state) and at 10 K (low-T state), i.e. well below the phase transition temperature, T_c. The low-T phase distinguishes itself from the high-T phase in transmission diffraction pattern in that it features a set of (3×3) periodic lattice distortion (PLD) peaks surrounding the fundamental Bragg peak as shown in Fig. 2. The emergence of these superlattice peaks are attributed to unit cell tripling along the b-axis and formation of trimer clusters of Ta atoms also along this axis as per our density functional theory (DFT) calculations (see Supplementary of ref. 16) and recent reports of low temperature structure of $TaTe_2$ using high-resolution scanning transmission electron microscopy (STEM) and related methods.[12,13,22,23] Therefore, these PLD superlattice peaks can be used as a sensitive marker of the newly formed trimer cluster phase of $TaTe_2$ and allows to visualize the photoinduced phase transition and hence, the melting of the emergent trimer atomic order using diffraction methods. This can be demonstrated by taking the difference between the patterns of the two phases as shown in Fig. 2b. The expected complete loss of the superlattice peaks occurs together with complex changes of fundamental Bragg peak intensities due to

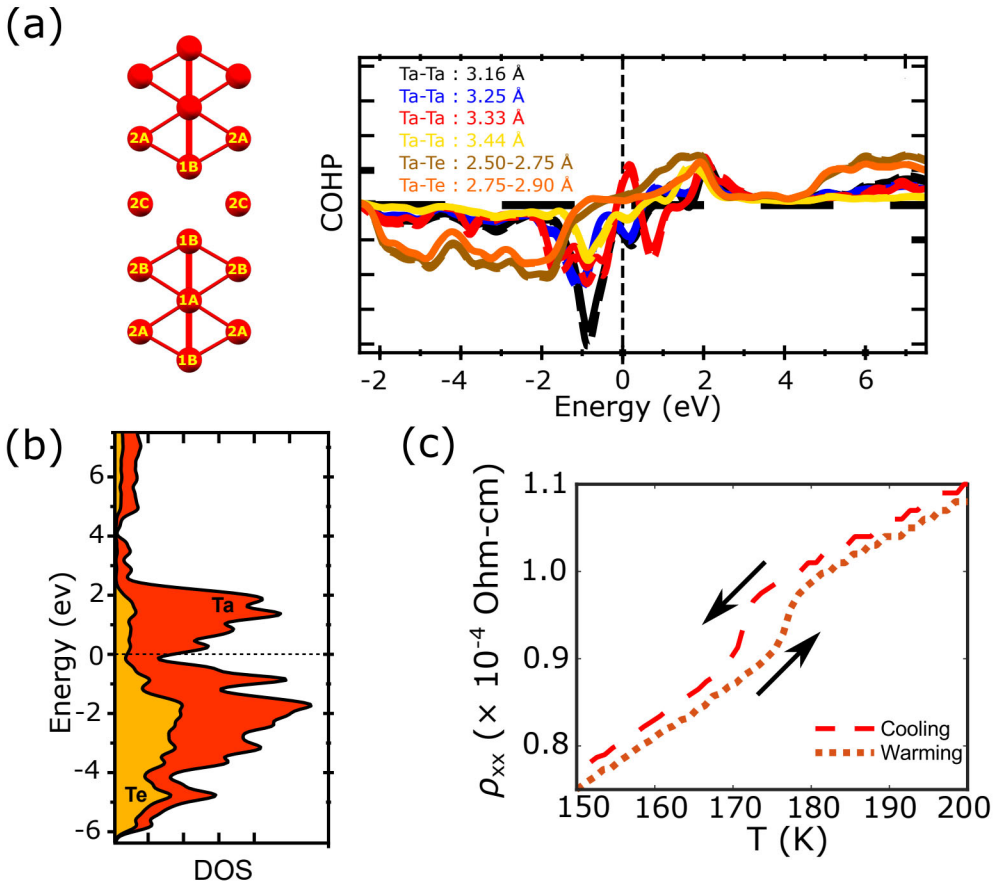

Figure 3. (a) Integrated crystal orbital Hamilton population (ICOHP) for low-T phase of $TaTe_2$ computed using DFT. Four non-equivalent Ta ions in the low-T phase along the zig-zag chain parallel to the b-axis are labelled. (b). Projected density of states of the low-T phase of $TaTe_2$. (c). In-plane resistivity of $TaTe_2$. The drop in resistivity at $\sim$ 175 K is consistent with a structural phase transition to a phase which is more metallic.

distorted monoclinic symmetry of the crystalline $TaTe_2$. Thus, the difference pattern in Fig. 2b is a signature that the phase transition has occurred in which the sample has been transformed into the high-T state.

We investigated the clustering of Ta atoms using DFT by examining the bonding nature between ions in the low-T phase by performing crystal orbital Hamilton population (COHP) analysis. This analysis can predict bonding or antibonding character of bonds by the sign of the integrated crystal orbital Hamilton population (ICOHP): negative for bonding and positive for antibonding. The results are shown in Fig. 3. The calculated ICOHP values for different bonds in the low-T phase are given in Table 1 and show negative values of ICOHP for bonds identified in Fig. 3a. Furthermore, the average Ta-Ta COHP along the b-axis axis in the low-T phase was found to have greater magnitude compared to the high-T phase (not shown). These observations predict stronger bonding between Ta atoms along the b-axis in the low-T phase resulting in them forming additional trimer clusters as found experimentally.

In addition, the projected density of the states (DOS) of the high-T and low-T phases were computed. It is shown for the trimer superstructure phase in Fig. 3b. The lower energy region of the valence band consists of contributions from p-orbitals of Te and d-orbitals of Ta with higher weights from the p-states of Te, whereas the region close to the Fermi level is mainly occupied by Ta states. The states in the conduction band near the Fermi level are attributed to non-bonding states of Ta trimers. The finite band overlap between the valence and conduction band suggests metallic behavior in the $TaTe_2$ low-T trimer state. Our calculations also found that the projected DOS at the Fermi level for low-T phase is larger than for high-T phase. Indeed, this is confirmed by in-plane resistivity measurement shown in Fig. 3c, which displays a drop in resistivity below the phase transition

temperature near 170 K denoted by the discontinuity, thus confirming that the system becomes more metallic in the low-T phase.

Table 1. Integrated COHP (ICOHP) between Ta atoms at the Fermi level calculated for the low-T structure. r_{bond} is the bond distance.

Bond type	r_{bond} (Å)	ICOHP
Ta(1A)-Ta(2A)	3.26	-0.957
Ta(1B)-Ta(2A)	3.16	-1.281
Ta(1B)-Ta(2B)	3.45	-0.622
Ta(1B)-Ta(1A)	3.33	-0.989
Ta(2A)-Ta(2A)	3.52	-0.693
Ta(2B)-Ta(2B)	3.68	-0.363
Ta(1B)-Ta(1B)	4.22	-0.020

3.2 Diffraction simulations

The origin of the observed changes in the difference pattern shown in Fig. 2b was investigated in terms of the atomic motions associated with the structural phase transition in $TaTe_2$ using multislice diffraction simulations.[24] Multislice methods were chosen due to presence of heavy elements ($Z_{Ta} = 73$ and $Z_{Te} = 52$) in $TaTe_2$ and high thickness of the sample as it can account for the multiple scattering effects which lead to non-trivial distribution of intensities in the diffraction pattern. For each calculation, we simulate plane-wave electron diffraction from a 60 nm thick $TaTe_2$ crystal at varying sample tilts covering the range observed in the AFM, then perform a weighted average of these simulated patterns to model diffraction from the rippled sample with a given tilt distribution (more details can be found in the Supplementary of ref. 16). The results are presented in Fig. 4. As illustrated in this figure, the diffraction simulations are performed starting with the trimer superstructure low-T phase and selectively moving either the Ta or Te sublattice in-plane towards the high-T phase. When one of the sublattices is moved, the other is kept frozen. The resulting pattern is then subtracted from the low-T phase diffraction pattern (Fig. 2b) and the difference compared to the signature of the phase transition. Qualitatively, the changes are well accounted for by motion of the Ta sublattice, which suggests that it is the motions of tantalum atoms that are dominating the phase transition in the plane.

3.3 Photoinduced phase transition

The phase transition from the trimer superstructure phase to the high-T phase was induced by pumping the system at 10 K with intense 1030 nm laser pulses. The photoinduced changes above the noise floor were only observed for the fluences > 1.5 mJ cm^{-2}, assigned as the threshold for onset of an optically-induced phase transition in our experiments. The temperature rise caused by the conversion of the absorbed laser energy into heat was estimated using the following expression:

$$\Delta T(K) = \frac{F_{abs}}{C_{\text{v}} d} \tag{1}$$

where, F_{abs} is the absorbed fluence, d is the sample thickness, and C_{v} is the temperature-dependent volumetric heat capacity reported in literature.[14] The calculated rise in temperature was found to fall in the range of 125-177 K for fluences used in this work. In Fig. 5b, the time traces of the superlattice peaks as a function of pump-probe delay for 2.3 mJ cm^2 are shown. The PLD peaks are seen to be suppressed by about 50% within the first 2 ps and then undergo a partial recovery. The delay-averaged difference pattern at early times is shown in Fig. 5a and strongly resembles the (low-T – high-T) pattern suggesting finite switching of the excited volume

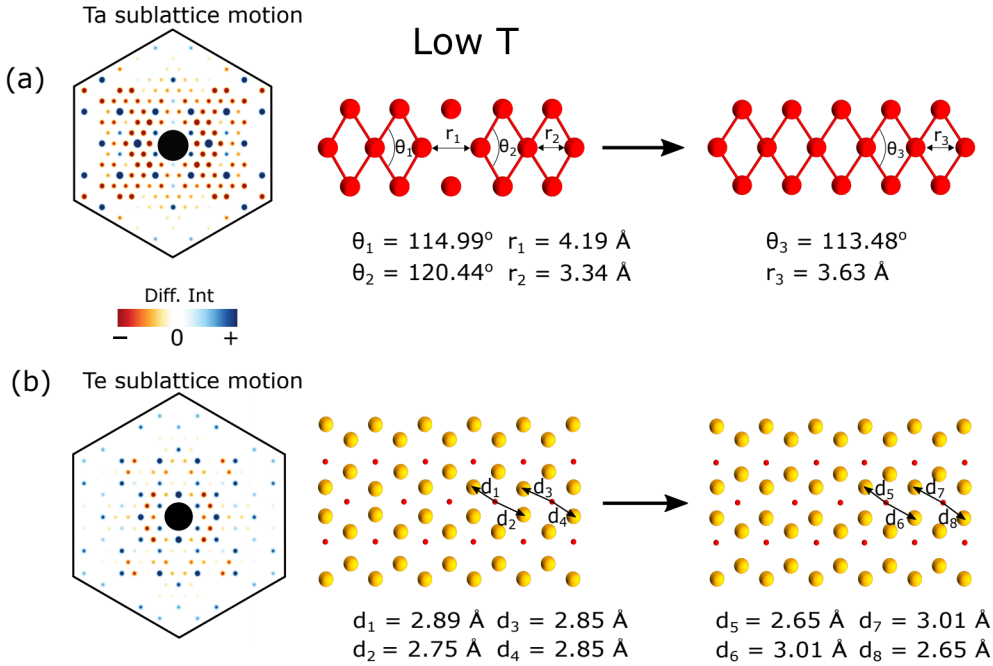

Figure 4. Simulated electron diffraction patterns using multislice simulations of $TaTe_2$. (a). Simulated pattern resulting from moving only the Ta sublattice towards the normal high-T state and the corresponding change in the geometry. (b). Simulated difference pattern obtained by subtracting the low-T diffraction pattern from that which results from moving only the Te sublattice towards the high-T state.

to the normal high-T phase. The data were fit to extract the time constants for both the decay and recovery of the PLD peaks using the following monoexponetial decay model:

$$F(t) = \left[\theta(t-t_0)\cdot[c1\cdot(1-\exp(-\frac{t-t_0}{\tau}))]+C\right] \circledast G \tag{2}$$

where $\theta(t-t_0)$ is the Heaviside step function, τ is the time constant, t_0 is time zero, c_1 and C are amplitude and constant offset, respectively. The model includes numerical convolution as denoted by operator $\circledast$ with a Gaussian function, G. The melting and partial recovery of the PLD peaks were found to occur with time constants of $\tau_{melt} = 1.44$ ps and $\tau_{rec} = 6.6$ ps. The changes of the fundamental Bragg peaks show the same mixed signs as the one observed in Fig. 2c, i.e. with some orders showing positive difference intensity while others display negative intensities. The recovered time constant for the fundamental Bragg peaks is about 2.3 ps.

The recovery of the PLD indicates that the system switches back into the low-T state with the trimer superstructure, but remains at elevated temperatures over several tens of picoseconds. This can seen in the delayed-averaged diffraction pattern in the middle panel of Fig. 5a in which nearly all the diffracted orders show a negative sign of intensity change due to higher temperature, which causes an increase of amplitude of the root-mean square atomic displacements, $< u^2 >$. Simulated Kinematical diffraction in which the Debye-Waller factor was increased by two times to generate a "hot" trimer superstructure state and then subtracted from the diffraction of the low-T state is shown in the right-most panel of Fig. 5a and corroborate this assertion.

4. SUMMARY

In summary, the experimental results of the time-resolved study of $TaTe_2$ are discussed. The experiments exploited ultrabright relativistic electrons from HiRES diffraction facility at LBNL to track the structural dynamics following melting of the PLD in $TaTe_2$. This versatile UED instrument provides opportunities for more detailed studies of structural dynamics in solids. For example, experiments with a single pulse up to 250 kHz repetition

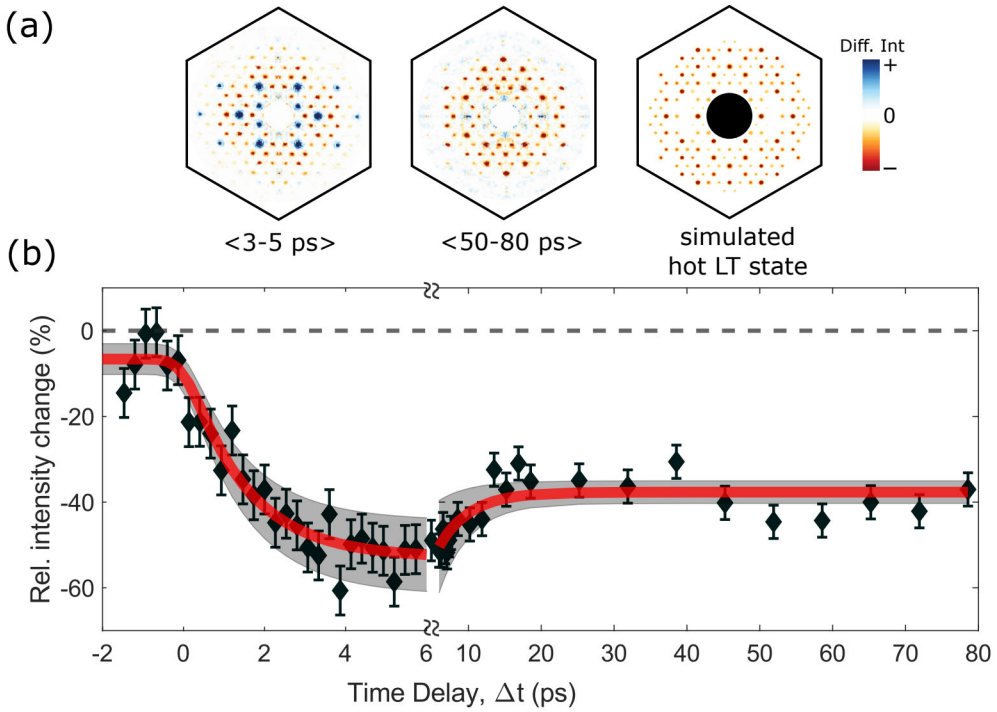

Figure 5. (a). Measured delay-averaged diffraction patterns for two time ranges and simulated Debye-Waller pattern of low-T $TaTe_2$. (b). Time trace of the PLD peaks showing a rapid suppression within 2 ps and subsequent recovery over several picoseconds. The fits are shown in red and 95% confidence bounds are also plotted.

rate are possible, which could be interesting for search of hidden metastable phases in quantum 2D materials using UED and monolayers or heterostructures which require high beam brightness to enhance the signal-to-noise, respectively. Thus, future work is expected to broaden the scope of solid state experiments to more complex systems at HiRES.

ACKNOWLEDGMENTS

We thank Nord Andresen of CXRO, LBNL for enormous help with design and installation of the cryostat and other engineering related contributions to HiRES beamline. K.M.S and R.A.K acknowledge support by the Laboratory Directed Research and Development (LDRD) Program of Lawrence Berkeley National Lab under U.S. Department of Energy (DOE) Contract DE-AC02-05CH11231. Funding for D.B.D. was provided by STROBE: A National Science Foundation Science and Technology Center under Grant No. DMR 1548924. D.F. would like to thank DOE for support under Contract DE-AC02–05CH11231 for development and operation of the HiRES instrument. Work at the Molecular Foundry was supported by the Office of Science, Office of Basic Energy Sciences, of the U.S. Department of Energy under Contract No. DE-AC02-05CH11231.

REFERENCES

[1] D. Basov, R. Averitt, and D. Hsieh, "Towards properties on demand in quantum materials," *Nature Materials* **16**(11), pp. 1077–1088, 2017.

[2] K. Khan, A. K. Tareen, M. Aslam, R. Wang, Y. Zhang, A. Mahmood, Z. Ouyang, H. Zhang, and Z. Guo, "Recent developments in emerging two-dimensional materials and their applications," *J. Mater. Chem. C* **8**, pp. 387–440, 2020.

[3] E. H. da Silva Neto, P. Aynajian, A. Frano, R. Comin, E. Schierle, E. Weschke, A. Gyenis, J. Wen, J. Schneeloch, Z. Xu, S. Ono, G. Gu, M. Le Tacon, and A. Yazdani, "Ubiquitous interplay between charge ordering and high-temperature superconductivity in cuprates," *Science* **343**(6169), pp. 393–396, 2014.

[4] M. Eichberger, H. Schäfer, M. Krumova, M. Beyer, J. Demsar, H. Berger, G. Moriena, G. Sciaini, and R. J. D. Miller, "Snapshots of cooperative atomic motions in the optical suppression of charge density waves," *Nature* **468**(7325), pp. 799–802, 2010.

[5] C. Paillard, E. Torun, L. Wirtz, J. Íñiguez, and L. Bellaiche, "Photoinduced phase transitions in ferroelectrics," *Phys. Rev. Lett.* **123**, p. 087601, 2019.

[6] J. Wang and S.-C. Zhang, "Topological states of condensed matter," *Nature Materials* **16**(11), pp. 1062–1067, 2017.

[7] N. Samarth, "Quantum materials discovery from a synthesis perspective," *Nature Materials* **16**(11), pp. 1068–1076, 2017.

[8] M. Rini, R. Tobey, N. Dean, J. Itatani, Y. Tomioka, Y. Tokura, R. W. Schoenlein, and A. Cavalleri, "Control of the electronic phase of a manganite by mode-selective vibrational excitation," *Nature* **449**, pp. 72–74, 2007.

[9] Y. Tokura, M. Kawasaki, and N. Nagaosa, "Emergent functions of quantum materials," *Nature Physics* **13**(11), pp. 1056–1068, 2017.

[10] L. Stojchevska, I. Vaskivskyi, T. Mertelj, P. Kusar, D. Svetin, S. Brazovskii, and D. Mihailovic, "Ultrafast switching to a stable hidden quantum state in an electronic crystal," *Science* **344**(6180), pp. 177–180, 2014.

[11] S. Kaiser, "Light-induced superconductivity in high-T_c cuprates," *Physica Scripta* **92**(10), p. 103001, 2017.

[12] H. Chen, Z. Li, L. Guo, and X. Chen, "Anisotropic magneto-transport and magnetic properties of low-temperature phase of $TaTe_2$," *EPL (Europhysics Letters)* **117**(2), p. 27009, 2017.

[13] C. Chen, H.-S. Kim, A. S. Admasu, S.-W. Cheong, K. Haule, D. Vanderbilt, and W. Wu, "Trimer bonding states on the surface of the transition-metal dichalcogenide $TaTe_2$," *Physical Review B* **98**(19), 2018.

[14] T. Sörgel, J. Nuss, U. Wedig, R. Kremer, and M. Jansen *Materials Research Bulletin* **41**(5), pp. 987 – 1000, 2006.

[15] A. Vernes, H. Ebert, W. Bensch, W. Heid, and C. Näther, "Crystal structure, electrical properties and electronic band structure of tantalum ditelluride," *Journal of Physics: Condensed Matter* **10**(4), pp. 761–774, 1998.

[16] K. M. Siddiqui, D. B. Durham, F. Cropp, C. Ophus, S. Rajpurohit, Y. Zhu, J. D. Carlström, C. Stavrakas, Z. Mao, A. Raja, P. Musumeci, L. Z. Tan, A. M. Minor, D. Filippetto, and R. A. Kaindl, "Ultrafast optical melting of trimer superstructure in layered 1 T'-$TaTe_2$," *arXiv:2009.02891* , 2020.

[17] D. Filippetto and H. Qian, "Design of a high-flux instrument for ultrafast electron diffraction and microscopy," *Journal of Physics B: Atomic, Molecular and Optical Physics* **49**(10), p. 104003, 2016.

[18] F. Ji, D. B. Durham, A. M. Minor, P. Musumeci, J. G. Navarro, and D. Filippetto, "Ultrafast Relativistic Electron Nanoprobes," *Communications Physics* **2**(1), 2019.

[19] R. J. D. Miller, "Femtosecond crystallography with ultrabright electrons and x-rays: Capturing chemistry in action," *Science* **343**(6175), pp. 1108–1116, 2014.

[20] A. Ubaldini, J. Jacimovic, N. Ubrig, and E. Giannini, "Chloride-driven chemical vapor transport method for crystal growth of transition metal dichalcogenides," *Crystal Growth & Design* **13**(10), pp. 4453–4459, 2013.

[21] A. Castellanos-Gomez, M. Buscema, R. Molenaar, V. Singh, L. Janssen, H. S. J. van der Zant, and G. A. Steele, "Deterministic transfer of two-dimensional materials by all-dry viscoelastic stamping," *2D Materials* **1**(1), p. 011002, 2014.

[22] I. El Baggari, N. Sivadas, G. M. Stiehl, J. Waelder, D. C. Ralph, C. J. Fennie, and L. F. Kourkoutis, "Direct visualization of trimerized states in 1 T'-$TaTe_2$," *Phys. Rev. Lett.* **125**, p. 165302, 2020.

[23] J. J. Gao, J. G. Si, X. Luo, J. Yan, F. C. Chen, G. T. Lin, L. Hu, R. R. Zhang, P. Tong, W. H. Song, X. B. Zhu, W. J. Lu, and Y. P. Sun, "Origin of the structural phase transition in single-crystal $TaTe_2$," *Phys. Rev. B* **98**, p. 224104, 2018.

[24] C. Ophus, "A fast image simulation algorithm for scanning transmission electron microscopy," *Advanced Structural and Chemical Imaging* **3**(1), 2017.